Frequency-domain multiplexing system for *in vivo* diffuse light measurements of rapid cerebral hemodynamics

Guoqiang Yu, Turgut Durduran, Daisuke Furuya, Joel H. Greenberg, and Arjun G. Yodh

A novel frequency-domain multiplexing system has been developed for *in vivo* measurements of rapid cerebral hemodynamics. The instrument operates in the frequency-domain with three optical wavelengths, six source positions, and two detectors. Frequency-division multiplexing was used to modulate three wavelengths (690, 786, and 830 nm) at slightly different frequencies around 70 MHz. The three laser output beams were combined and switched into different source positions by use of fast optical switches (switch time <10 ms). Three narrowband, in-phase and in-quadrature demodulators decode the modulated signals. Our full-frame-acquisition rate is 2.5 Hz, with flexibility for acquisition rates greater than 50 Hz with smaller detection areas. We evaluate the performance of the instrument with tissue phantoms, and then employ the system to measure *in vivo* cerebral blood oxygenation during forepaw stimulation of a rat's brain. © 2003 Optical Society of America

OCIS codes: 170.0110, 170.3660, 170.3890, 170.5380, 170.6960, 170.5270.

1. Introduction

Near-infrared (NIR) light provides an attractive means for noninvasive monitoring of tissue absorption and scattering. Diffuse optical tomography (DOT), for example, employs multiple wavelengths in the NIR to derive low-resolution images of total hemoglobin concentration (HbT), tissue blood oxygen saturation (StO2), and other tissue optical properties that can be related to metabolic activity.

Recently, there has been growing interest in NIR methods for investigation of brain activation in animal models[1–5] and humans[6–10] during various stimulation paradigms. NIR spectroscopy and its imaging mode, DOT, are proving suitable for these measurements as a low-cost, portable, and flexible modality that complements methods such as functional magnetic resonance imaging.[11–13] The diffuse optical scheme holds promise for fundamental stud-ies of neurovascular activity in animal models and for bedside monitoring of humans.

To achieve this promise it is desirable to obtain high spatial resolution images rapidly at several optical wavelengths. Speed is required to observe the rapid spatiotemporal metabolic activity in the brain. Provocation by exercise,[14] vasoactive agents,[15] and electrical stimulation[16] can produce flow changes in the cerebral vasculature within a few seconds or less. Moreover, the microvascular perfusion of tissue exhibits significant spatial and temporal variations even at rest.[17] Instruments with high temporal resolution permit the measurement of these rapid changes, but, as always, there is a trade-off between spatial, spectral, and temporal resolution.

In the past, we have developed several instruments for DOT and for blood flow measurements. For example, we have recently built a hybrid instrument that combines two NIR diffuse optical techniques; diffuse photon density wave (DPDW) spectroscopy for total hemoglobin concentration and oxygenation, and diffuse correlation flowmetry for cerebral blood flow (CBF). Time-division multiplexing (TDM) was employed to optically switch 4 wavelengths and 12 source positions consecutively. The instrument required 2.5 min to obtain one image; 1.5 min for the DCS measurement with one wavelength (800 nm) and four detectors; and one min for the DPDW measurement with three wavelengths, 12 source posi-

Guoqiang Yu (guoqiang@physics.upenn.edu), T. Durduran, and A. G. Yodh are with the Department of Physics and Astronomy, and D. Furuya and J. H. Greenberg are with the Department of Neurology, Cerebrovascular Research Center, University of Pennsylvania, Philadelphia Pennsylvania 19104.

tions, and 4 detectors. We employed this hybrid instrument to measure *in vivo* cerebral HbT, StO2, and CBF dynamics of a rat's brain during hypercapnia, hypoxia, cardiac arrest, and ischemia.[18–22] The instrument was appropriate for monitoring slow dynamic processes but was unable to monitor fast metabolic activities such as the rapid changes of oxyhemoglobin (HbO2) and deoxyhemoglobin (Hbr) concentration in the rat somatosensory cortex during periodic electrical forepaw stimulation. The primary concern addressed in this paper is improved fast NIR spectroscopic imaging.

Three major experimental techniques are currently employed for these types of experiments. Continuous-wave (cw) spectroscopy is the simplest technique, but separation of absorption and scattering can be difficult with amplitude information only.[23,24] The main advantage of the cw system is its ability to achieve high frame rates. Time-resolved systems (TRSs) and frequency-domain DOT systems contain more information per source–detector pair, since they measure the amplitude and temporal delay or phase shift. The additional information facilitates better separation of absorption and scattering. TRSs have potentially the highest information content, but they require significant averaging time to optimize the signal-to-noise ratio (SNR).[25,26] For example, a TRS with 32 source positions, 32 parallel detection channels, and 2 wavelengths requires 10 to 20 min to acquire one image frame.[26] Frequency-domain systems are low-cost alternatives to the more expensive TRSs, and can have superior stability over time while still allowing for separation of absorption and scattering changes. Frequency-domain systems were shown to be capable of reconstruction images of absolute scattering and absorption for better quantification of tissue physiology. However, most of the current imaging instruments in the frequency domain for DOT feature relatively long acquisition times (more than 30 s).[5,7,27]

TDM can be used to encode each source, detector, or wavelength and thus performs many measurements nearly simultaneously to increase the data-acquisition rate. Franceschini *et al.*[28] reported a fast imaging system in the frequency domain with 8 source positions, 2 detectors, and 2 wavelengths in which 16 laser diodes were used. Sixteen laser diodes (two wavelengths) were electronically time-division multiplexed at a rate of 100 Hz (10 ms on time per diode), yielding a frame-acquisition time of 160 ms (6.25 Hz). Wolf *et al.*[29] have recently reported a fast instrument that works in the frequency domain with four source positions, four detectors, and one wavelength and that utilizes the TDM method to change the source positions. The sample rate for one frame was 96 Hz in this case.

To reduce the image-acquisition time even further, several groups have employed frequency-division multiplexing (FDM) instead of the TDM to access source positions, wavelengths, or both in their cw systems.[30–32] Siegel *et al.*[31] used the FDM technique to derive one cw image with eight source positions, eight detectors, and two wavelengths in 0.5 s (2 Hz). Schmitz *et al.*[32] developed a similar cw instrument that provides one image with 25 source positions, 32 detectors, and 1–4 wavelengths in 0.37 s (2.7 Hz).

Thus far only one instrument in the frequency domain has employed FDM. Yang *et al.*[33] described a dual-wavelength homodyne system that employs the FDM method to determine the optical properties of tissue. They tested this system using Intralipid and ink, and they evaluated the accuracy of the instrument *in vitro* for determining hemoglobin saturation at a rate of one data point per minute with a single source–detector separation. The spatial, spectral, and temporal resolutions of their system were inadequate for *in vivo* DOT imaging. Nevertheless, they demonstrated that the FDM technique could reduce the measuring time for frequency-domain devices significantly, at the cost of moderate increased expense and complexity.

In this paper, we introduce a combination of TDM and FDM to acquire rapid images in the frequency domain. The FDM coding of spectral wavelength has no temporal skew; errors typically caused by channel-to-channel delay in the case of the TDM are reduced, and the acquisition time is significantly shortened. We then combine this method with TDM to optimize instrument size and cost through sharing of detection electronics, electronic switches, and fast optical switches. In this paper, we describe an extensive characterization of a prototype (Generation I) instrument. The Generation I device operated with three wavelengths, six source positions, and two detectors, achieving a full-frame rate of 2.5 Hz with adequate SNR during *in vivo* measurements of rat brain stimulation. This device enabled us to rapidly localize the activation region and then carry out higher-speed (20 Hz) measurements using one source and two detectors. We stress the flexibility and modularity of the instrument by outlining a method to increase the number of sources and detectors while keeping relatively high frame-acquisition rates. Using this basic approach, we have recently built a Generation II system with 5 wavelengths, 16 source positions, and 4 detector channels multiplexed to 8 detectors. We have also characterized this system, albeit to a much lesser degree than Generation I. We report its dynamic range and noise-equivalent power (NEP). Finally, a comparison of DOT instruments in the frequency domain is given.

2. Instrument Design

A. Frequency-Division Multiplexing Method

A schematic of our FDM system is shown in Fig. 1. The FDM method simultaneously codes for three laser diodes operating at 690, 786, and 830 nm respectively. Each wavelength operates continuously, but at slightly different modulation frequencies ω_1, ω_2, and ω_3 around 70 MHz with modulation frequency differences of ~30 kHz. The modulated light sources are combined and introduced into the turbid
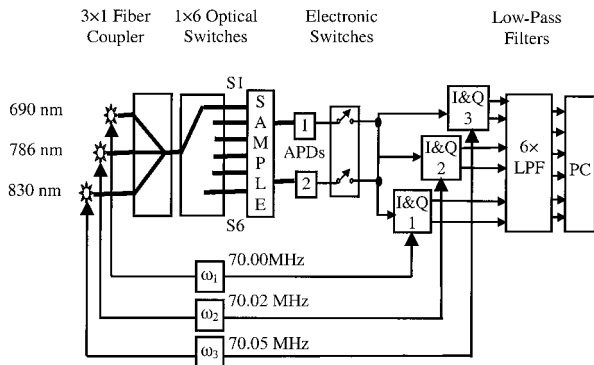
Fig. 1. FDM system with three wavelengths (690, 786, and 830 nm), six source positions (S1, S2, . . . and S6), and two detectors (D1 and D2). Three oscillators (ω_1, ω_2, and ω_3) drive three laser diodes and provide the reference signals to three demodulators (I&Q 1, I&Q 2, and I&Q 3).

medium by optical fibers. The reflected or transmitted light from the turbid medium contains three signals and is detected by an avalanche photodiode (APD). Three in-phase and in-quadrature (I&Q) demodulators working at center frequencies ω_1, ω_2, and ω_3, are used to decode the superimposed signals in parallel. Two low-pass filters with an 80-Hz cutoff frequency were used to obtain the dc components, in-phase $I_{i-dc} = A_i \cos(\theta_i)$ and in-quadrature $Q_{i-dc} = A_i \sin(\theta_i)$, from the outputs of the demodulators. Here $i = 1$–3 represent particular wavelengths, θ_i is the phase shift, and A_i is the ac amplitude of the measured DPDW. The amplitudes and phases of the DPDW can then be determined[34]:

$$A_i = (Q_{i-dc}{}^2 + I_{i-dc}{}^2)^{1/2}, \qquad (1)$$

$$\theta_i = \tan^{-1}(Q_{i-dc}/I_{i-dc}). \qquad (2)$$

The DPDW amplitudes and phases are then analyzed to extract bulk optical properties (μ_s' and μ_a) or their spatial distribution. Here μ_a is the absorption coefficient and μ_s' is the reduced scattering coefficient. Use of multiple wavelengths and the extinction coefficient spectra of tissue chromophores such as HbO2 and Hbr enable us to compute blood oxygen saturation and HbT.

B. Hemoglobin Concentrations and Image Reconstruction

In this paper, we employ a method that directly fits for the hemoglobin concentrations using *a priori* information about their spectra. We have previously shown that this approach reduces the interparameter cross talk and therefore improves quantitative information.[35] We normalize the data with the baseline amplitude and phase, and we assume baseline blood oxygen saturation, HbT, and scattering values from the literature of 50%, 100 μM, and 15 cm^{-1}, respectively.[4,36,37] This process allows us to obtain relative

changes in chromophore concentrations. In the calculation, we define and minimize

$$\chi^2 = \sum \|\Phi_m(t)/\Phi_m(t_0) - \Phi_c(t)/\Phi_c(t_0)\|^2.$$

Here $\Phi_m(t)$ is the measured fluence and $\Phi_c(t)$ is the calculated fluence at time (t). They are normalized by the baseline fluence at time $t = t_0$. The sum is over the source–detector pairs and all wavelengths. The calculated fluence is determined with a semi-infinite model at the fitted values of a given iteration. We use the Nelder–Mead simplex (direct search) method implemented in the MATLAB function "fminsearch" to fit for the unknowns by minimizing χ^2. We then calculate blood saturation and HbT from the relevant hemoglobin concentrations. We have also investigated the dependence of the fitted results on assumed baselines over a large range (e. g., blood oxygen saturation was varied between 40% and 80%). The relative concentration changes depended minimally on the assumed baseline values over the physiologically expected range.

Differential image reconstructions were obtained with a linear Rytov approximation approach with Tikhonov regularization. Only intensity data was employed to reconstruct absorption perturbations at each wavelength.[38] These low-resolution images enable us to localize the strongest response to forepaw stimulation.

C. Instrumentation

Figure 1 shows a diagram of the instrument. The instrument represents a compromise between temporal and spatial resolution. Based on these considerations as well as circuit simplicity, cost, and instrument size we combined the FDM and TDM methods.

With the FDM method, three low-noise rf signal oscillators (70 MHz, 13 dB; Wilmanco, Ventura, California), drive three laser diodes, 690 nm (HL6738MG, 30 mW; Hitachi, Tokyo, Japan), 786 nm (DL7140-201, 70 mW; Sanyo Semiconductors, Richmond, Indiana), and 830nm (HL8325G, 40 mW; Hitachi, Tokyo, Japan) at slightly different modulation frequencies (70.00 MHz, 70.03 MHz, and 70.05 MHz). The modulated light is combined and switched into six source positions by an optical fiber coupler (C_TM-DL-01-0410-85-FC/FC; FOCI Fiber Optic Communications, Hsinchu, Taiwan) and several fast optical switches (1 × 4 Prism switch, switch time <10 ms; Dicon Fiberoptics, Richmond, California) (TDM method). The signal from each of the two APD's (C5331-03; Hammamatsu, Bridgewater, New Jersey) is alternately switched to I&Q demodulators by means of electronic switches (8000 serials/DIP Reed Relay, switch time <0.5 ms; Coto Technology, Providence, Rhode Island) to reduce detection hardware costs and instrument dimensions. Each channel consists of three narrowband I&Q demodulators (MIQY-70D; Minicircuits, Brooklyn, New York) to decode the three modulated signals. A pair of low-pass filters with a cutoff frequency of 80 Hz are connected

Table 1. Performance Characteristics of the Generation I System

Parameter	Value
NEP	2 pW (rms)
Dynamic range	>70 dB: amplitude errors $< \pm 1$ %, phase error $<1°$
Interchannel cross talk	< -40 dBmV
Long-term stability	Amplitude errors $< \pm 1$ % and phase error $<1°$ in 30 min
Temporal response	80 Hz

with the output of each I&Q demodulator to filter out all high-frequency signals. The six channel signals (one detector channel $\times$ three decoders $\times$ two) are then digitized by a 16-channel 16-bit data-acquisition board (PCI-6032E; National Instrument, Austin, Texas). One frame (three wavelengths, six source positions, and two detectors) with signal averaging times of 20 ms can be obtained in less than 0.4 s with this new instrument. The data-acquisition time per source–detector per wavelength of this instrument is a factor of 50 times shorter than that of our previous device.[18] The hardware was modularized according to function; for example, the lasers, detectors, switches, I&Q, and low-pass filters, were kept in different nuclear instrumentation boxes (NIM BIN). NIM BIN modules adequately isolated rf signals, keeping the instrument noise low. This design also provides flexibility for enlarging the number of source–detector pairs in the system by increasing the APDs and optical switches.

3. Evaluation of System Performance

A. Instrument Performance Characteristics

The experimental evaluation of the Generation I system performance is shown in Table 1. The offset and offset noise in this type of rf circuitry are derived from the voltage readout when no sources were turned on.

The offset noise (~ 5 μV) was minimized by careful shielding of all the components. An offset of <1 mV was measured at the beginning of each frame and subtracted from the signal. The NEP was determined by converting the offset noise level to units of power by use of the measured linearity curve.

Measuring the dynamic range of the instrument required attachment of a variable optical attenuator to the source fiber, and the amplitude and phase of the transmitted DPDW through a tissue phantom was recorded while the source strength decreased. The power was measured with an optical powermeter. This measurement was done for powers ranging from well above saturation to deep into the noise. The dynamic range of the system consisted of the following: the region where the deviation of amplitude is less than ± 1 % and the phase error is less than $1°$ from the least-squares-fit line. Figure 2 shows one measurement of the dynamic range (amplitude only, at *786* nm). The voltage range (amplitude in vertical axis) defines the dynamic range (>70 dB).

Interchannel cross talk was measured by looking at the largest change among the other channels while one single channel was driven across the whole dynamic range. The long-term stability measurement was taken on a static and homogeneous phantom for 30 min.

Results shown in Table 1 indicate we were able to achieve good system performance characteristics. Our NEP (NEP $= 2$ pW) is reasonable compared with the specified NEP of the APDs. A dynamic range of >70 dB is similar to other instruments[18] and is adequate for imaging the rat brain with our source–detector arrangement (<50 dB, refer to Fig. 3). The interchannel cross talk of <40 dBmV is much less than the expected signal variations resulting from rat brain activation, and is therefore sufficient to achieve adequate SNR. The long-term stability of the in-
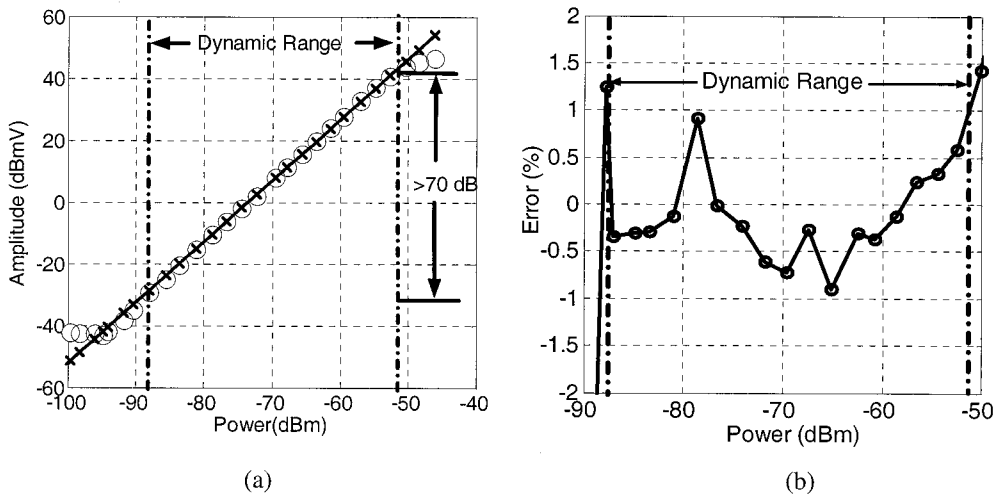
Fig. 2. (a) Dynamic range test result (measured amplitude versus power through medium) for the 786-nm wavelength (only amplitude is shown); noise level: <-40 dBmV; saturation level: 40 dBmV; dynamic range: >70 dB (amplitude in vertical axis). (b) Percent deviation of amplitude from a least-squares-fit line (is less than $\pm 1\%$).
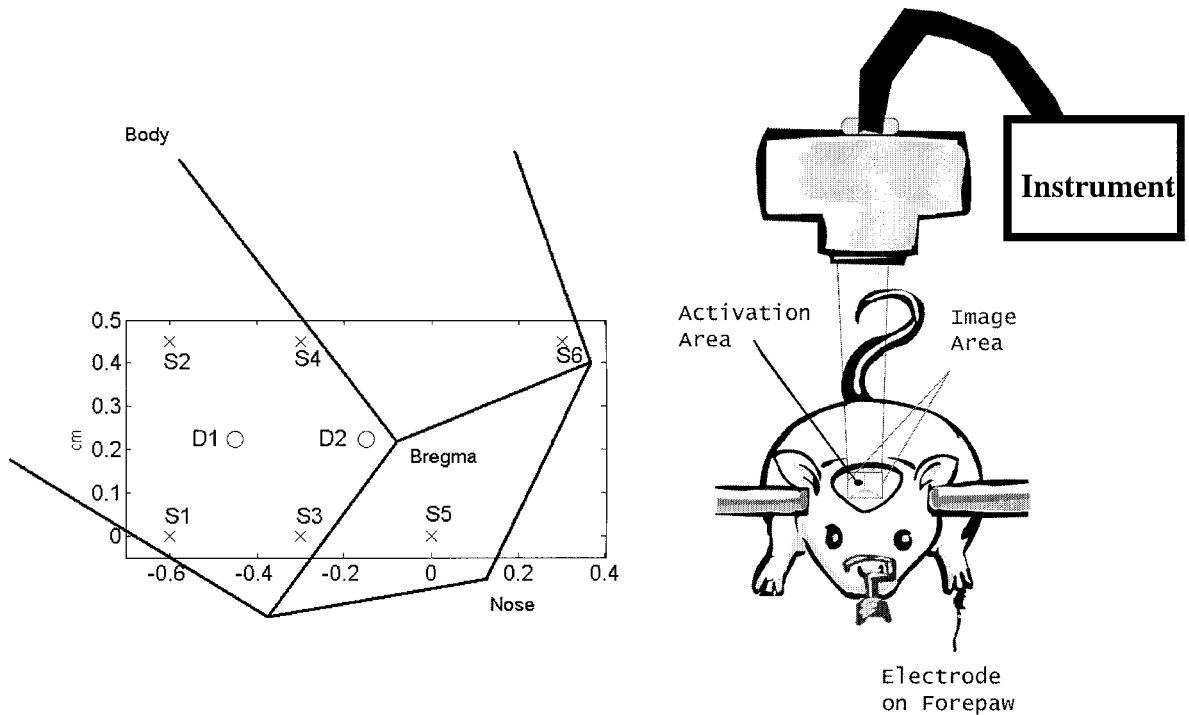
Fig. 3. Scheme for measuring the HbO2 and Hbr concentrations in a rat's somatosensory cortex during periodic electrical forepaw stimulation. The left part of the figure shows the optical probe map over the brain (depicted with dark solid lines) with six source positions (S1 to S6) and two detectors (D1 and D2).

strument is attractive since some studies require continuous long-time data acquisition. The temporal response is adequate for most measurements and can be improved by trading off with increased noise.

B. *In vivo* Measurements of Somatosensory Cortex Activation by Forepaw Stimulation on rat brains

To verify the system efficacy *in vivo,* we used the instrument to measure blood oxygen changes in the rat somatosensory cortex during periodic electrical forepaw stimulation. The arrangement of the measurement system is shown in Fig. 3.

Adult rats (300–350 g) were anesthetized with halothane (1% to 1.5%) in a mixture of 70% nitrous oxide and 30% oxygen. An arterial catheter was inserted to monitor the blood pressure and heart rate and a catheter was inserted into the femoral vein for drug delivery. The body temperature was maintained at 37 °C with a temperature-controlled heating pad. After a tracheostomy, the animal was placed on a mechanical ventilator, and the head was secured in a stereotaxic frame to reduce motion artifacts. The scalp was reflected to avoid the fur-induced distortion onto the NIR signals. After the surgical procedures, halothane was withdrawn and anesthesia was maintained with α-chloralose (60 mg/kg), followed by supplemental dose of 30 mg/kg every hour. A periodic electrical stimulation signal (5 Hz, 2.0 mA) was applied to the median nerve between the forepaw to produce a localized neuronal activation of the brain. The source (*cross*) and detector (*circle*) optical fibers assembled on a noncontact probe were

arranged in a two-dimensional planar pattern as shown in the left part of the Fig. 3.

Initially, measurements were taken at 2.5 Hz (frame-acquisition rate) with six source positions and two detectors. A series of images were obtained to locate the response area stimulated by forepaw stimulation. Figure 4 shows three images of relative absorption coefficient changes at 690 nm before (−4 s), during (5 s at peak response), and after (25 s) forepaw stimulation (8-s stimulus duration with an intrastimulus time of 30 s). The images show that the response area is at the area around the source position 4 (S4) and the two detectors (D1 and D2). When the source–detector pair was identified with a strong differential signal, further measurements were taken at 20 Hz with that source position and two detectors (i.e., S4, D1, and D2, ~3 mm apart). Measurements at three wavelengths (690, 786, and 830 nm) were used to extract hemoglobin concentrations and blood oxygen saturation by means of the method discussed above.

Figure 5(a) shows the relative concentration changes of the HbO$_2$ and Hbr, and Fig. 5(b) shows the relative concentration changes of the HbT, induced by a series of stimulations. The stimulus duration was 8 s with an intrastimulus time of 30 s. The stimulus frequency was 5 Hz at 2 mA. Data was collected at 20 Hz with one source and two detectors (S4, D1, and D2). The corresponding change of StO2 is shown in Fig. 5(c). During the stimulation, the HbT increased 5–7 μM from baseline, whereas the StO2 increased 9%– 11% relative to baseline. The
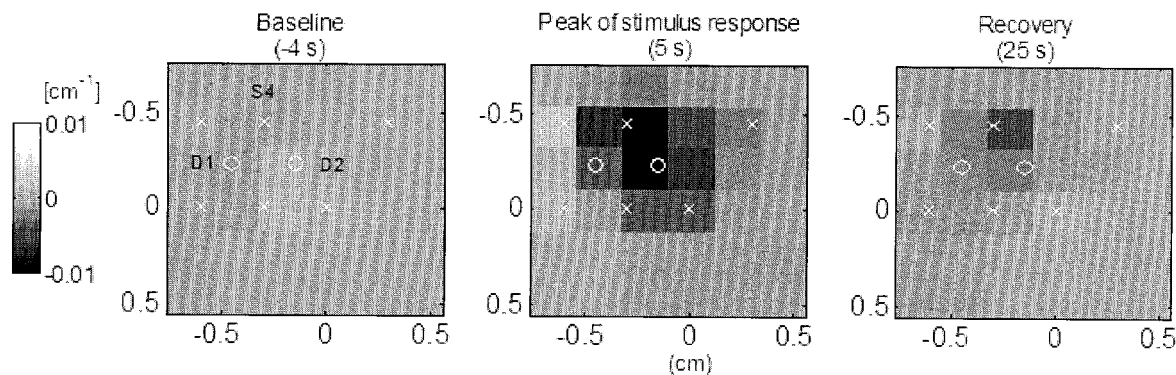
Fig. 4. Two-dimensional images of relative absorption coefficient-at 690 nm are reconstructed 2 mm below the top of the skull. A decrease in absorption at 690 nm (due to a decrease in deoxyhemoglobin concentration) is apparent in the middle image (S4, D1, and D2), taken at peak of stimulus response (5 s after stimulus onset). Left and right images correspond to baseline (-4 s) and recovery (25 s) periods, where $t = 0$ is the stimulus onset. Circles represent detector positions, and crosses represent source positions.

average half-width half-maximum of the peaks was 4.5 s. The short-duration, small-amplitude response signal induced by forepaw stimulation required the measurement system's high sampling rate, low-noise, and long-term stability. The results shown in Fig. 5 demonstrate that our instrument was able to achieve good SNR (SNR >10) and dynamic sampling (20 Hz).

We also measured the relative change of StO2 during periodic forepaw stimulation of either 8 or 4 s. Figure 6 shows changes of StO2 induced by two different stimulus durations (8 or 4 s). Data was collected at 20 Hz with one source and two detectors (S4, D1, and D2). The average delay to response, defined as the latency from stimulus onset to initial response, was 2 s for both of the two stimulation series. Note that longer stimulation (8 s) causes an activation response consisting of an initial peak followed by a plateau, whereas the 4 s stimulation led to a peak response only. Increasing the duration of stimulation to 60 s produces a more prolonged response with a distinctive initial peak, followed by a plateau that slowly decreases toward the baseline level during the second half of the stimulation period (not shown). These temporal characteristics demonstrate the temporal resolution of our device and are consistent with studies in which laser Doppler[39] and O$_2$ microelectrodes are used.[40] Our probe, of course, provides spatial information too, an important advantage for DOT.

4. Summary and Discussion

A. Summary

We have demonstrated a fast, low-cost, multiwavelength, multi–source–detector Generation I diffuse optical tomography system in the frequency domain combining frequency-division-multiplexing and TDM techniques. The combination of two multiplexing methods and the modularity of hardware provide us with flexibility to trade-off measurement time, number of source–detector pairs, and cost.
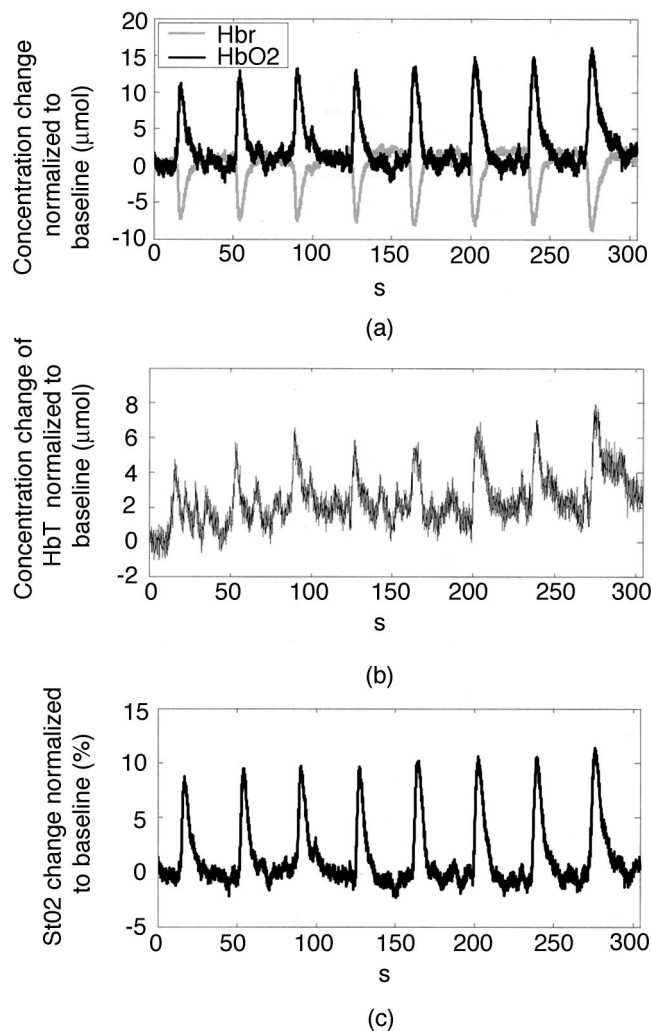
Fig. 5. (a) Concentration changes (relative to baseline) of HbO2 and Hbr for the serial stimulation. (b) Relative concentration changes of HbT. (c) Percent changes (relative to baseline) of StO2. The stimulus duration was 8 s with an intrastimulus time of 30 s; stimulus frequency was 5 Hz at 2 mA. The sampling rate was 20 Hz with one source and two detectors (S4, D1, and D2). StO2 is given in percentage and concentrations are given in micromole.
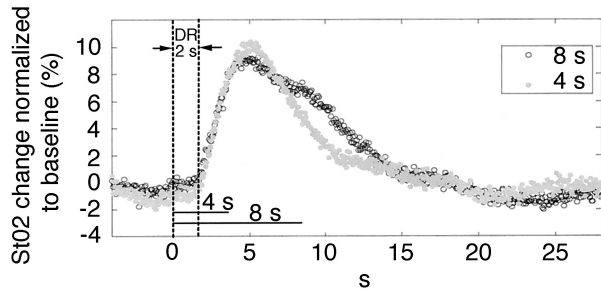
Fig. 6. StO2 changes for 8 s (open circles) or 4 s (solid dots) of forepaw stimulation with 30-s or 34-s interstimulus interval. Stimulus frequency was 5 Hz at 2mA. The sampling rate was 20 Hz with one source and two detectors (S4, D1, and D2).

B. Outline of a Higher Temporal and Spatial Imaging System (Generation II)

The modular instrument design makes possible the enlargement of our current system. Having successfully built and evaluated the instrument discussed above, we are now developing imaging systems with higher temporal and spatial resolution. Our Generation II system combines FDM and TDM into one instrument with 5 wavelengths, 16 source positions, and 8 detectors operating in the frequency domain.[41] With the FDM method, five wavelengths (675, 786, 830, 860, and 980 nm) are modulated at five different frequencies, whereas with the TDM method, the modulated light is switched into 16 source positions by optical switches. Four detector channels are multiplexed to eight fiber-coupled APDs by use of eight electronic switches (TDM) to cut down detection hardware costs and instrument dimensions. Each detection channel consists of five narrowband I&Q

demodulators to decode the five modulated signals. The total 40 channel signals (4 detector channels $\times$ 5 decoders $\times$ 2) are collected by a 64-channel 16-bit data-acquisition board. One frame (5 wavelengths, 16 source positions, and 8 detectors) with signal averaging times of the order 20 ms can be obtained in less than 1 s (1 Hz). This novel design provides great flexibility to balance the temporal resolution and spatial resolution as source–detector pairs can be easily selected by software without changing any hardware. Table 2 lists different possible temporal and spatial resolutions achieved by the Generation II system. The highest data-acquisition rate depends on the measurement time for each source–detector pair and on the temporal response of the system (80 Hz). To reduce the noise level and increase the dynamic range of the current instrument, we use 20 ms (dwell time) to average the detected signal for each source–detector pair; thus, the highest data-acquisition rate of our instrument is 50 Hz. The design is very modular, allowing addition and removal of sources, detectors, and wavelengths by simple swapping of different NIM BINs.

We evaluated the performance of the Generation II system using the same method as described for Generation I, and we achieved similar results shown in Table 1: the NEP <10 pW, dynamic range >70 dB, interchannel cross talk <−40 dBmV. The instrument is further optimized and animal studies are underway for *in vivo* verification of the system efficacy.

C. Comparison of Some Instruments for Diffuse Optical Tomography

Many groups have attempted to get DOT images with high temporal and spatial resolution. Some characteristics of recent instruments in the frequency domain are listed in Table 3. We use data points (source numbers $\times$ detector numbers $\times$ wavelengths) and data-acquisition rate (data points per second) to characterize spatial, spectral, and temporal resolution.

Comparing the instruments shown in Table 3, it can be seen that the instruments by Wolf *et al.*[29] (1536 Hz), Franceschni *et al.*[28] (200 Hz) and Yu *et al.*[41] (90 Hz) can be used for monitoring rapid processes in the brain. Note that the dwell time of our

Table 2. Temporal, Spectral, and Spatial Resolutions of the Generation II System

Number of Wavelengths	Number of Source Positions	Number of Detectors	Data-Acquisition Rate (Hz)
5	1	4	50.0
5	1	8	25.0
5	9	4	2.50
5	16	8	1.00
5	45	24	0.16

Table 3. Comparison of Some Instruments for DOT in Frequency Domain Recently Reported

Systems	McBride *et al.*[27,a]	Yu *et al.*[41] Generation I	Franceschni *et al.*[28]	Yu *et al.*[41] Generation II	Wolf *et al.*[29]
Source number	16	6	8	16	4
Detector number	16	2	2	8	4
Wavelength number	5	3	2	5	1
Data points	1280	36	32	640	16
Acquisition time (s)	30	0.4	0.16	1	0.011
Data rate (Hz)	42	90	200	640	1536
Multiplexing method	TDM	TDM + FDM	TDM	TDM + FDM	TDM

[a]Dwell time is much larger than 20 ms because source–detector separations are larger for breast measurements. All of the other instruments are designed for the brain and thus have shorter dwell time.

instrument for each source–detector pair was 20 ms, more than double that of the other two instruments. For greater spatial and spectral resolution, the instrument of McBride *et al.*[27] (1280 data points) and our Generation II system (640 data points)[41] with 16 source positions, 8 detectors, and 5 wavelengths, are much higher than others. The data-acquisition rate of our Generation II system (640 Hz) is 15 times higher than that of McBride *et al.*[27] (42 Hz, see footnote in Table 3 about this comparison).

References

1. I. Oda, Y. Wada, S. Takeuchi, Y. Oikawa, N. Sakauchi, Y. Ito, I. Konishi, Y. Tsunazawa, T. Kusaka, K. Isobe, S. Itoh, and S. Onishi, "Near-infrared optical imager for cerebral blood flow and oxygenation detection," in *Optical Tomography and Spectroscopy of Tissue IV,* B. Chance, R. R. Alfano, B. J. Tromberg, M. Tamura, and E. M. Sevick-Muraca, eds., Proc. SPIE **4250,** 371–379 (2001).

2. S. Fantini, D. Hueber, M. A. Franceschini, E. Gratton, W. Rosenfeld, P. G. Stubblefield, D. Maulik, and M. R. Stankovic, "Non-invasive optical monitoring of the newborn piglet brain using continuous-wave and frequency-domain methods," Phys. Med. Biol. **44,** 1543–1563 (1999).

3. D. A. Boas, T. J. Gaudette, G. Strangman, X. Cheng, J. A. Marota, and J. B. Mandeville, "The accuracy of near infrared spectroscopy and imaging during focal changes in cerebral hemodynamics," Neuroimage **13,** 76–90 (2001).

4. M. Jones, J. Berwick, D. Johnston, and J. Mayhew, "Concurrent optical imaging spectroscopy and laser-Doppler flowmetry: the relationship between blood flow, oxygenation, and volume in rodent barrel cortex," Neuroimage **13,** 1002–1015 (2001).

5. R. M. Danen, Y. Wang, X. D. Li, W. S. Thayer, and A. G. Yodh, "Regional imager for low-resolution functional imaging of the brain with diffusing near-infrared light," Photochem. Photobiol. **67,** 33–40 (1998).

6. A. Villringer, J. Planck, C. Hock, L. Schleinkofer, and U. Dirnagl, "Near infrared spectroscopy (NIRS): a new tool to study hemodynamic changes during activation of brain function in human adults," Neurosci. Lett. **154,** 101–104 (1993).

7. B. Chance, E. Anday, S. Nioka, S. Zhou, L. Hong, K. Worden, C. Li, T. Murray, Y. Ovetsky, D. Pidikiti, and R. Thomas, "A novel method for fast imaging of brain function, non-invasively, with light," Opt. Express **2,** 411–423 (1998), http://www.opticsexpress.org/abstract.cfm?URI=OPEX-2-10-411

8. A. Duncan, J. H. Meek, M. Clemence, C. E. Elwell, L. Tyszczuk, M. Cope, and D. T. Delpy, "Optical pathlength measurements on adult head, calf and forearm and the head of the newborn infant using phase resolved optical spectroscopy," Phys. Med. Biol. **40,** 295–304 (1995).

9. J. Steinbrink, M. Kohl, H. Obrig, G. Curio, F. Syre, F. Thomas, H. Wabnitz, H. Rinneberg, and A. Villringer, "Somatosensory evoked fast optical intensity changes detected non-invasively in the adult human head," Neurosci. Lett. **291,** 105–108 (2000).

10. S. R. Hintz, D. A. Benaron, A. M. Siegel, A. Zourabian, D. K. Stevenson, and D. A. Boas, "Bedside functional imaging of the premature infant brain during passive motor activation," J. Perinat Med. **29,** 335–343 (2001).

11. J. B. Mandeville and J. Marota, "Vascular filters of functional MRI: spatial localization using BOLD and CBV contrast," Magn. Reson. Med. **42,** 591–598 (1999).

12. T. Q. Duong, D. S. Kim, K. U. Urbil, and S. G. Kim, "Spatio-temporal dynamics of the BOLD fMRI signals: toward mapping submillimeter cortical columns using the early negative response," Magn. Reson. Med. **44,** 231–242 (2002).

13. N. Vasilis, A. G. Yodh, M. Schnall, X. H. Ma, and B. Chance, "Calculation of local optical properties in highly scattering media using *a-priori* structural information for application to simultaneous NIR-MR breast examination," in *Photon Propagation in Tissues IV,* D. A. Benaron, B. Chance, M. Ferrari, eds., Proc. SPIE **3566,** 200–206 (1998).

14. C. R. Honig, C. L. Odoroff, and J. L. Frierson, "Capillary recruitment in exercise: rate, extent, uniformity and relation to blood flow," Am. J. Physiol. **238,** H31–H42 (1980).

15. Y. Kakihana, M. M. Kessler, A. Krug, H. Yamada, T. Oda, and N. Yoshimura, "Dynamic changes in intracapillary hemoglobin oxygenation in human skin following various temperature changes," Microvasc. Res. **56,** 104–112 (1998).

16. B. M. Ances, J. A. Detre, K. Takahashi, and J. H. Greenberg, "Transcranial laser Doppler mapping of activation flow coupling of the rat somatosensory cortex," Neurosci. Lett. **257,** 25–28 (1998).

17. R. B. King, G. M. Raymond, and J. B. Bassingthwaighte, "Modeling blood flow heterogeneity," Ann. Biomed. Eng. **24,** 352–372 (1996).

18. C. Cheung, J. P. Culver, K. Takahashi, J. H. Greenberg, and A. G. Yodh, "*In vivo* cerebrovascular measurement combining diffuse near-infrared absorption and correlation spectroscopies," Phys. Med. Biol. **46,** 2053–2065 (2001).

19. J. P. Culver, T. Durduran, D. Furuya, C. Cheung, J. H. Greenberg, and A. G. Yodh, "Diffuse optical measurement of hemoglobin and cerebral blood flow in rat brain during hypercapnia, hypoxia and cardiac arrest," in *Advances in Experimental Medicine and Biology, Oxygen Transport to Tissue Volume XXIII,* D. F. Wilson, S. M. Evans, J. Biaglow, A. Pastuszko, eds. (Plenum, 2002), pp. 293–298.

20. J. P. Culver, C. Cheung, T. Durduran, D. Furuya, J. H. Greenberg, and A. G. Yodh, "Diffuse optical tomography of hemoglobin concentrations, and cerebral blood flow in rat brain during focal ischemia," in *Digest of OSA Biomedical Topical Meetings,* (Optical Society of America, Washington, D.C., 2002), pp. 170–172.

21. T. Durduran, G. Yu, J. P. Culver, C. Cheung, D. Furuya, J. H. Greenberg, and A. G. Yodh, "Hemodynamics of cortical spreading depression and forepaw stimulation," in *Digest of OSA Biomedical Topical Meetings* (Optical Society of America, Washington, D.C., 2002), pp. 164–166.

22. T. Durduran, G. Yu, J. P. Culver, C. Cheung, D. Furuya, J. H. Greenberg, and A. G. Yodh, "Brain hemodynamics and oxygen metabolism: hybrid approach," in in *Digest of OSA Biomedical Topical Meetings* (Optical Society of America, Washington, D.C., 2002), pp. 47–49.

23. S. R. Arridge and W. R. B. Lionheart, "Non-uniqueness in diffusion-based optical tomography," Opti. Lett. **23,** 882–884 (1998).

24. S. R. Arridge, "Optical tomography in medical imaging," Inverse Probl. **15,** R41–R93 (1999).

25. V. Ntziachristos, X. Ma, and B. Chance, "Time-correlated single photon counting imager for simultaneous magnetic resonance and near infrared mammography," Rev. Sci. Instrum. **69,** 4221–4233 (1998).

26. F. E. W. Schmit, M. E. Fry, E. M. C. Hillman, J. C. Hebden, and D. T. Delpy," A 32-channel time-resolved instrument for medical optical tomography," Rev. Sci. Instrum. **71,** 256–265 (2000).

27. T. O. McBride, B. W. Pogue, S. D. Jiang, and U. L. Osterberg, "A parallel-detection frequency-domain near-infrared tomog-

raphy system for hemoglobin imaging of the breast *in vivo,*" Rev. Sci. Instrum. **72,** 1817–1824 (2001).

28. M. A. Franceschini, V. Toronov, M. E. Filiaci, E. Gratton, and S. Fantini, "On-line optical imaging of the human brain with 160-ms temporal resolution," Opt. Express **6,** 49–57 (2000), http://www.opticsexpress.org/abstract.cfm?URI=OPEX-6-3-49.

29. M. Wolf, U. Wolf, J. H. Choi, L. P. Safonova, R. Gupta, V. Toronov, A. Michalos, L. A. Paunescu, and E. Gratton, "Functional fast neuronal signals in the visual and motor cortex detected by frequency-domain near-infrared spectroscopy," in *Digest of OSA Biomedical Topical Meetings* (Optical Society of America, Washington, D.C., 2002) pp. 205–207.

30. H. Koizumi, A. Maki, and T. Yamamoto, "Optical tomography: practical problems and novel applications," in *Digest of OSA Biomedical Topical Meetings* (Optical Society of America, Washington, D.C., 2002), pp. 294–296.

31. A. M. Siegel, J. J. A. Marota, and D. A. Boas, "Design and evaluation of a continuous-wave diffuse optical tomography system," Opt. Express **4,** 287–298 (1999), http://www.opticsexpress.org/abstract.cfm?URI=OPEX-4-8-287.

32. C. H. Schmitz, M. Locker, J. Mlasker, A. H. Hielscher, and R. L. Barbour, "Instrumentation for fast functional optical tomography," Rev. Sci. Instrum. **73,** 1–11 (2002).

33. Y. Yang, H. L. Liu, X. D. Li, and B. Chance, "Low cost frequency-domain photon migration instrument for tissue spectroscopy, oximetry, and imaging," Opt. Eng. **36,** 1562–1569 (1997).

34. Mini-Circuits Division of Scientific Components, RF/IF De-signer's Handbook (Scientific Components, Mini-Circuits, New York, 1997).

35. T. Durduran, R. Choe, J. P. Culver, L. Zubkov, M. J. Holboke, J. Giammarco, B. Chance, and A. G. Yodh, "Bulk optical properties of healthy female breast tissue," Phys. Med. Biol. **47,** 2847–2862 (2002).

36. J. Mayhew, D. Johnston, J. Martindale, M. Jones, J. Berwick, and Y. Zheng, "Increased oxygen consumption following activation of brain: theoretical footnotes using spectroscopic data from barrel cortex," Neuroimage **13,** 975–987 (2001).

37. W. F. Cheong, S. A. Prahl, and A. J. Welch, "A review of optical properties of biological tissues," IEEE J. Quantum Electron. **26,** 2166–2185 (1990).

38. A. C. Kak and M. Slaney, *Principles of Computerized Tomographic Imaging* (IEEE Press, New York, 1988).

39. J. A. Detre, B. M. Ances, K. Takahashi, and J. H. Greenberg, "Signal averaged laser Doppler measurements of activation-flow coupling in the rat forepaw somatosensory cortex," Brain Res. **796,** 91–98 (1998).

40. B. M. Ances, D. G. Buerk, J. H. Greenberg, and J. A. Detre, "Temporal dynamics of the partial pressure of brain tissue oxygen during functional forepaw stimulation in rats," Neurosci. Lett. **306,** 106–110 (2001).

41. G. Yu, T. Durduran, D. Furuya, R. Choe, J. H. Greenberg, and A. G. Yodh, "Frequency domain diffuse optical multiplexing system for rapid hemodynamics," in *Digest of OSA Biomedical Topical Meetings* (Optical Society of America, Washington, D.C., 2002), pp. 184–186.